AIAA SciTech Forum
January 3-7, 2022, San Diego, CA & Virtual
AIAA SCITECH 2022 Forum

10.2514/6.2022-1377

Minimum Time-of-Flight Interceptor Guidance Using Real-Time-Implementable Model-Predictive Guidance

Syed Aseem Ul Islam * and Dennis S. Bernstein †
University of Michigan, Ann Arbor, MI, 48109

This paper presents a model-predictive guidance law for planar interception that minimizes the miss distance and time-of-flight in order to achieve sub-optimal real-time implementable guidance. This guidance law is designed with fixed-computational complexity to facilitate real-time implementation. Furthermore, scenario specifics, such as pursuer and evader types, can be specified and are used by the guidance law to compute a solution at each step.

I. Introduction

Missile guidance remains a highly important and challenging problem. Challenges arise from the nonlinear dynamics of the pursuer, including constraints on thrust and turn rate, as well as uncertainty about the ability of the evader to maneuver. The widely studied proportional guidance (PG) law [1, Chapter 6], [2, 3] is suited to a wide variety of applications. PG is derived using constant speed assumptions for both the pursuer and the evader within the context of a kinematic engagement [1, pp 14–18] model. Another advantage of PG is that it is computationally cheap to implement. These assumptions are reasonable for short segments of or short engagements, such as terminal phase, or for special cases where the pursuer is travelling significantly faster than the evader. However, the assumptions underlying PG are are violated in meaningful ways in many real-world guidance applications. In particular, the constant speed assumption is violated due to attitude and altitude dependent drag affect the flight of long range missiles that operate within the atmosphere such as medium- and long-range air-to-air missiles. Furthermore, variations in thrust as a function of speed, time, and altitude also affect the speeds of the pursuer and evader. Consequently, the trajectories flown by medium- and long-range air-to-air missiles are designed based on the need to conserve kinetic energy, and thus PG is not suitable for these applications. Augmented proportional guidance (APG) [1, p.165], [4] is an extension of PG that accounts for maneuvering targets by requiring measurements or estimates of target acceleration. However, APG is based on the same assumptions as PG, which are violated in significant ways during many real-world engagements.

Optimal control concepts have been used to derive guidance laws [5–9]. These guidance laws are derived by solving optimization problems based on simplified engagement dynamics that do not consider the aerodynamics of the pursuer or the evader. Furthermore, since guidance laws need to be real-time implementable on hardware, these guidance laws are based on suboptimal solutions. [8] takes into account the aerodynamics of the pursuer to derive an LQG-based guidance law. There has also been recent interest in polynomial guidance laws [10–12], which assume that the guidance law is given by a polynomial function of the time-to-go.

A promising approach to guidance is model predictive control (MPC), which uses the available model and receding horizon optimization to determine a future sequence of control inputs subject to actuation constraints, such as magnitude and rate saturation [13–16]. The ability of MPC to handle nonlinear dynamics, actuation constraints, and knowledge of the desired trajectory make this approach a viable candidate for guidance [17–19]. An important advantage of MPC is its ability to use knowledge of the dynamics of the pursuer and evader for computing an optimal trajectory. Knowledge of the dynamics of the pursuer is available to the designer of the guidance law for the pursuer, and knowledge of the dynamics of the evader is often available to the pursuer through non-cooperative target recognition [20–23]. Noncooperative target recognition is the process of determining the pursuer type based on analysis of radar, infrared, or other types of returns. A challenge in the implementation of MPC is computational complexity due to the requirement to solve an optimization problem, which may be nonlinear.

The main contribution of this paper is the development of a minimum-time planar model-predictive guidance (MPG) law for a beyond-visual-range (BVR) air-to-air missile that takes into account aerodynamic and atmospheric effects, as well as the pursuer flight characteristics. That is, the guidance law can be adapted to different types of pursuers. A minimum-time engagement is desirable since missiles are limited by the amount of time for which they can provide thrust. Furthermore, due to the "shrinking-horizon" utilized by this MPG law, it is applicable to midcourse, terminal,

*Research Scholar, Aerospace Engineering, 1320 Beal Ave, Ann Arbor, MI, USA.
†Professor, Aerospace Engineering, 1320 Beal Ave, Ann Arbor, MI, USA.

and endgame segments of the engagement, which precludes hand-off constraints that are associated with midcourse guidance. Moreover, the procedure presented in this paper can be extended to include additional dynamic effects and 3d interception dynamics without modification of the optimization procedure. This gives MPG a large potential for extensions that include additional effects and for different applications. That is, this paper provides a framework for MPG using air-to-air missile guidance as an example, which can be modified and extended based on specific applications. The derivation of the engagement dynamics and the MPG law is presented in a tutorial fashion in order to facilitate readers new to the topic to understand and replicate the results. Since MPG utilizes a model-predictive framework, constraints on the normal acceleration of the missile are incorporated into the optimization algorithm. Furthermore, MPG is able to utilize information about target maneuvers if it is available.

The contents of this paper as as follows. Section II presents the planar engagement dynamics that form the basis of MPG. Section III presents MPG. In particular, numerical methods for gradient computation and discretization of the nonlinear engagement dynamics are presented, which are used for prediction and optimization. A method for input-constrained nonlinear optimization using Nesterov's accelerated gradient descent is presented. Finally, aerodynamic models for the pursuer and evader used in this paper are presented. Section IV presents augmented proportional guidance and Section V presents numerical examples that investigate the application of MPG in various scenarios. Finally, section VI provides concluding remarks and directions for future research.

II. Engagement Dynamics

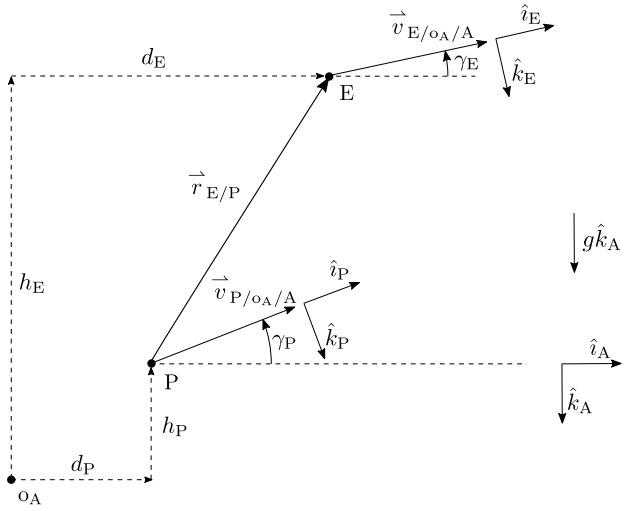

Fig. 1 Planar interception geometry for the pursuer and evader. The inertial frame $\mathrm{F_A}$ is defined by the unit vectors $\hat{\imath}_{\mathrm{A}}, \hat{k}_{\mathrm{A}}$. The pursuer P and evader E are at altitudes h_{P} m and h_{E} m, respectively, relative to $\mathrm{o_A}$, which is a fixed point at sea level. P and E are distances d_{P} m and d_{E} m downrange, respectively. The unit vectors $\hat{\imath}_{\mathrm{P}}$ and $\hat{\imath}_{\mathrm{E}}$ are aligned with the velocity vectors $\vec{v}_{\mathrm{P/o_A/A}}$ and $\vec{v}_{\mathrm{E/o_A/A}}$, respectively. The gravity vector $g\hat{k}_{\mathrm{A}}$ affects all motion.

Consider a pursuer P and evader E, with position vectors $\vec{r}_{\mathrm{P/o_A}}$ and $\vec{r}_{\mathrm{E/o_A}}$, respectively, where $\mathrm{o_A}$ is a reference point with zero inertial acceleration, as shown in Figure 1. Let the pursuer and evader speeds V_{P} and V_{E} in m/s, respectively, be given by

$$V_{\mathrm{P}} \triangleq |\vec{v}_{\mathrm{P/o_A/A}}|, \quad V_{\mathrm{E}} \triangleq |\vec{v}_{\mathrm{E/o_A/A}}|. \tag{1}$$

Let $\mathrm{F_P}$ and $\mathrm{F_E}$ be frames whose x-axes are aligned with the velocity vectors of the pursuer and evader, respectively, and thus

$$\vec{v}_{\mathrm{P/o_A/A}} = V_{\mathrm{P}}\hat{\imath}_{\mathrm{P}}, \tag{2}$$

$$\vec{v}_{\mathrm{E/o_A/A}} = V_{\mathrm{E}}\hat{\imath}_{\mathrm{E}}, \tag{3}$$

and

$$\mathrm{F_A} \xrightarrow[2]{\gamma_\mathrm{P}} \mathrm{F_P}, \quad \mathrm{F_A} \xrightarrow[2]{\gamma_\mathrm{E}} \mathrm{F_E}, \tag{4}$$

where γ_P and γ_E are the pursuer and evader flight-path angles in rad, respectively, and

$$\vec{\omega}_{\mathrm{P/A}} = \dot{\gamma}_\mathrm{P}\hat{\jmath}_\mathrm{P}, \quad \vec{\omega}_{\mathrm{E/A}} = \dot{\gamma}_\mathrm{E}\hat{\jmath}_\mathrm{E}, \tag{5}$$

in rad/s. Taking the time derivative of (2) and (3) with respect to the $\mathrm{F_A}$ frame and using (5) yields

$$\vec{a}_{\mathrm{P/o_A/A}} \triangleq \overset{\mathrm{A}\bullet}{\vec{v}}_{\mathrm{P/o_A/A}} = \dot{V}_\mathrm{P}\hat{\imath}_\mathrm{P} + V_\mathrm{P}\overset{\mathrm{A}\bullet}{\hat{\imath}_\mathrm{P}} = \dot{V}_\mathrm{P}\hat{\imath}_\mathrm{P} + V_\mathrm{P}(\vec{\omega}_{\mathrm{P/A}} \times \hat{\imath}_\mathrm{P}) = \dot{V}_\mathrm{P}\hat{\imath}_\mathrm{P} - V_\mathrm{P}\dot{\gamma}_\mathrm{P}\hat{k}_\mathrm{P}, \tag{6}$$

$$\vec{a}_{\mathrm{E/o_A/A}} \triangleq \overset{\mathrm{A}\bullet}{\vec{v}}_{\mathrm{E/o_A/A}} = \dot{V}_\mathrm{E}\hat{\imath}_\mathrm{E} + V_\mathrm{E}\overset{\mathrm{A}\bullet}{\hat{\imath}_\mathrm{E}} = \dot{V}_\mathrm{E}\hat{\imath}_\mathrm{E} + V_\mathrm{E}(\vec{\omega}_{\mathrm{E/A}} \times \hat{\imath}_\mathrm{E}) = \dot{V}_\mathrm{E}\hat{\imath}_\mathrm{E} - V_\mathrm{E}\dot{\gamma}_\mathrm{E}\hat{k}_\mathrm{E}. \tag{7}$$

respectively.

Next, we model the forces on the pursuer and the evader. For this paper we include the effects of uniform gravity, simplified aerodynamic drag, and normal acceleration on the pursuer and evader. Based on the requirements of a particular application, additional effects can be included at this stage of the derivation. Let the acceleration of the pursuer and evader be given by

$$\vec{a}_{\mathrm{P/o_A/A}} = \left(\tfrac{T_\mathrm{P} - D_\mathrm{P}}{m_\mathrm{P}} - g\sin\gamma_\mathrm{P}\right)\hat{\imath}_\mathrm{P} + (n_{z,\mathrm{P}} + g\cos\gamma_\mathrm{P})\hat{k}_\mathrm{P}, \tag{8}$$

$$\vec{a}_{\mathrm{E/o_A/A}} = \left(\tfrac{T_\mathrm{E} - D_\mathrm{E}}{m_\mathrm{E}} - g\sin\gamma_\mathrm{E}\right)\hat{\imath}_\mathrm{E} + (n_{z,\mathrm{E}} + g\cos\gamma_\mathrm{E})\hat{k}_\mathrm{E}, \tag{9}$$

respectively, where $T_\mathrm{P}, D_\mathrm{P}, m_\mathrm{P}, n_{z,\mathrm{P}}$ and $T_\mathrm{E}, D_\mathrm{E}, m_\mathrm{E}, n_{z,\mathrm{E}}$ are the thrust force in N, drag force in N, mass in kg, and normal acceleration of the pursuer and evader in $\mathrm{m/s^2}$, respectively. Note that (8) and (9) express the accelerations of the pursuer and evader due to thrust, drag, and gravitational acceleration, respectively. Thrust and drag models that take into account the angle of attack may be included in (8) and (9) but are omitted since their inclusion would require measurements or estimation of the angle-of-attack of the pursuer and evader. Note that in (8) and (9) we assume that thrust and drag forces act exclusively in the axial direction, whereas the normal acceleration acts in the normal direction by definition. It follows from (7)–(9) that

$$\dot{V}_\mathrm{P} = \tfrac{T_\mathrm{P} - D_\mathrm{P}}{m_\mathrm{P}} - g\sin\gamma_\mathrm{P}, \tag{10}$$

$$\dot{V}_\mathrm{E} = \tfrac{T_\mathrm{E} - D_\mathrm{E}}{m_\mathrm{E}} - g\sin\gamma_\mathrm{E}, \tag{11}$$

$$\dot{\gamma}_\mathrm{P} = -\tfrac{1}{V_\mathrm{P}}(n_{z,\mathrm{P}} + g\cos\gamma_\mathrm{P}), \tag{12}$$

$$\dot{\gamma}_\mathrm{E} = -\tfrac{1}{V_\mathrm{E}}(n_{z,\mathrm{E}} + g\cos\gamma_\mathrm{E}). \tag{13}$$

Assuming that the angle of attack is zero, the drag force in N on the pursuer and evader are given by

$$D_\mathrm{P} = \tfrac{1}{2}\rho(h_\mathrm{P})V_\mathrm{P}^2 S_\mathrm{P} C_{\mathrm{d,P}}(\mathrm{M_P}), \tag{14}$$

$$D_\mathrm{E} = \tfrac{1}{2}\rho(h_\mathrm{E})V_\mathrm{E}^2 S_\mathrm{E} C_{\mathrm{d,E}}(\mathrm{M_E}), \tag{15}$$

respectively, where $\rho(h_\mathrm{P})$, $\rho(h_\mathrm{E})$ and $\mathrm{M_P}$, $\mathrm{M_E}$ are the densities in $\mathrm{kg/m^3}$ and Mach numbers at altitudes h_P m and h_E m, respectively, as given by the international standard atmosphere (ISA). Note that the Mach number M at the altitude h is given by $\mathrm{M}(h) = \frac{V}{a(h)}$, where V is the speed and $a(h)$ is the speed of sound at the altitude h. Next, note that

$$\dot{h}_\mathrm{P} = V_\mathrm{P}\sin\gamma_\mathrm{P}, \quad \dot{d}_\mathrm{P} = V_\mathrm{P}\cos\gamma_\mathrm{P}, \tag{16}$$

$$\dot{h}_\mathrm{E} = V_\mathrm{E}\sin\gamma_\mathrm{E}, \quad \dot{d}_\mathrm{E} = V_\mathrm{R}\cos\gamma_\mathrm{E}. \tag{17}$$

Finally, using (10)–(17) we can express the engagement dynamics as

$$\dot{x} = f(x, u, w, t), \tag{18}$$

$$R = h(x), \tag{19}$$

where

$$x \triangleq \begin{bmatrix} V_{\mathrm{P}} \\ \gamma_{\mathrm{P}} \\ h_{\mathrm{P}} \\ d_{\mathrm{P}} \\ V_{\mathrm{E}} \\ \gamma_{\mathrm{E}} \\ h_{\mathrm{E}} \\ d_{\mathrm{E}} \end{bmatrix}, \quad f(x,u,w,t) \triangleq \begin{bmatrix} \frac{T_{\mathrm{P}} - \frac{1}{2}\rho(h_{\mathrm{P}})V_{\mathrm{P}}^2 S_{\mathrm{P}} C_{\mathrm{d,P}}(\mathrm{M_P})}{m_{\mathrm{P}}} - g\sin\gamma_{\mathrm{P}} \\ -\frac{1}{V_{\mathrm{P}}}(n_{z,\mathrm{P}} + g\cos\gamma_{\mathrm{P}}) \\ V_{\mathrm{P}}\sin\gamma_{\mathrm{P}} \\ V_{\mathrm{P}}\cos\gamma_{\mathrm{P}} \\ \frac{T_{\mathrm{E}} - \frac{1}{2}\rho(h_{\mathrm{E}})V_{\mathrm{E}}^2 S_{\mathrm{E}} C_{\mathrm{d,E}}(\mathrm{M_E})}{m_{\mathrm{E}}} - g\sin\gamma_{\mathrm{E}} \\ -\frac{1}{V_{\mathrm{E}}}(n_{z,\mathrm{E}} + g\cos\gamma_{\mathrm{E}}) \\ V_{\mathrm{E}}\sin\gamma_{\mathrm{E}} \\ V_{\mathrm{E}}\cos\gamma_{\mathrm{E}} \end{bmatrix}, \quad w \triangleq n_{z,\mathrm{E}}, \quad u \triangleq n_{z,\mathrm{P}}, \tag{20}$$

$$R = h(x) \triangleq \sqrt{(h_{\mathrm{E}} - h_{\mathrm{P}})^2 + (d_{\mathrm{E}} - d_{\mathrm{P}})^2}, \tag{21}$$

where R is the range from the pursuer to the evader and the magnitude of the line-of-sight vector $\vec{r}_{\mathrm{E/P}}$ in m. We define the evader normal acceleration $n_{z,\mathrm{E}}$ to be a disturbance to be rejected and the pursuer normal acceleration $n_{z,\mathrm{P}}$ to be the control variable.

For realism we assume that $|n_{z,\mathrm{E}}| < 8\,\mathrm{g}$ and $|n_{z,\mathrm{P}}| < 40\,\mathrm{g}$, where g is the acceleration due to gravity in $\mathrm{m/s^2}$. We assume that T_{P} and T_{E} are given either as lookup tables or functions. Note that forms of T_{P} and T_{E} may be modified based on application requirements. We will assume that the functional form of T_{E} is known through noncooperative target recognition. For example, if the target is a specific fighter jet, then T_{E} may be selected to be it's maximum thrust setting as a function of its altitude h_{E}. $\rho(h)$ is the density of air at altitude h given by the international standard atmosphere (ISA). The drag coefficients $C_{\mathrm{d,P}}(\mathrm{M_P})$ and $C_{\mathrm{d,E}}(\mathrm{M_E})$ are functions of Mach number. We will assume that $C_{\mathrm{d,P}}(\mathrm{M_P})$ is known to the designer of the missile through modeling and that $C_{\mathrm{d,E}}(\mathrm{M_E})$ is available through noncooperative target recognition.

We will assume that measurements of the entire state x are available to the missile, either through to its own seeker or through a data-link with a parent aircraft. Furthermore, we will assume that the missile seeker provides measurements R.

A. Change of Coordinates

Note that the variables that define the state x typically have numerical values whose magnitudes are different by orders of 10. For example, at some time the state might have the value

$$x = \begin{bmatrix} V_{\mathrm{P}} & \gamma_{\mathrm{P}} & h_{\mathrm{P}} & d_{\mathrm{P}} & V_{\mathrm{E}} & \gamma_{\mathrm{E}} & h_{\mathrm{E}} & d_{\mathrm{E}} \end{bmatrix}^{\mathrm{T}} = \begin{bmatrix} 900 & 0.05 & 12000 & 0 & 500 & -0.11 & 15000 & 60000 \end{bmatrix}^{\mathrm{T}}, \tag{22}$$

Thus, for better numerical conditioning of the dynamics simulation we define

$$\overline{V}_{\mathrm{P}} \triangleq \tfrac{1}{1000}V_{\mathrm{P}}, \quad \overline{V}_{\mathrm{E}} \triangleq \tfrac{1}{1000}V_{\mathrm{E}}, \quad \bar{h}_{\mathrm{P}} \triangleq \tfrac{1}{1000}h_{\mathrm{P}}, \quad \bar{h}_{\mathrm{E}} \triangleq \tfrac{1}{1000}h_{\mathrm{E}}, \quad \bar{d}_{\mathrm{P}} \triangleq \tfrac{1}{1000}d_{\mathrm{P}}, \quad \bar{d}_{\mathrm{E}} \triangleq \tfrac{1}{1000}d_{\mathrm{E}}, \tag{23}$$

where $\overline{V}_{\mathrm{P}}, \overline{V}_{\mathrm{E}}, \bar{h}_{\mathrm{P}}, \bar{h}_{\mathrm{E}}, \bar{d}_{\mathrm{P}}, \bar{d}_{\mathrm{E}}$ are the pursuer and evader speeds in km/s, altitudes in km, and downrange distances in km, respectively. Using the definitions (23) we can express the dynamics (18), (19) as

$$\dot{\bar{x}} = \bar{f}(\bar{x}, u, w, t), \tag{24}$$

$$R = \bar{h}(\bar{x}), \tag{25}$$

where

$$\bar{x} \triangleq \begin{bmatrix} \overline{V}_{\mathrm{P}} \\ \gamma_{\mathrm{P}} \\ \bar{h}_{\mathrm{P}} \\ \bar{d}_{\mathrm{P}} \\ \overline{V}_{\mathrm{E}} \\ \gamma_{\mathrm{E}} \\ \bar{h}_{\mathrm{E}} \\ \bar{d}_{\mathrm{E}} \end{bmatrix}, \quad \bar{f}(\bar{x}, u, w, t) \triangleq \begin{bmatrix} \frac{T_{\mathrm{P}} - \frac{1}{2}\rho(\bar{h}_{\mathrm{P}})(1000\overline{V}_{\mathrm{P}})^2 S_{\mathrm{P}} C_{\mathrm{d,P}}(\mathrm{M_P})}{1000 m_{\mathrm{P}}} - \frac{g}{1000}\sin\gamma_{\mathrm{P}} \\ -\frac{1}{1000\overline{V}_{\mathrm{P}}}(n_{z,\mathrm{P}} + g\cos\gamma_{\mathrm{P}}) \\ \overline{V}_{\mathrm{P}}\sin\gamma_{\mathrm{P}} \\ \overline{V}_{\mathrm{P}}\cos\gamma_{\mathrm{P}} \\ \frac{T_{\mathrm{E}} - \frac{1}{2}\rho(\bar{h}_{\mathrm{E}})(1000\overline{V}_{\mathrm{E}})^2 S_{\mathrm{E}} C_{\mathrm{d,E}}(\mathrm{M_E})}{1000 m_{\mathrm{E}}} - \frac{g}{1000}\sin\gamma_{\mathrm{E}} \\ -\frac{1}{1000\overline{V}_{\mathrm{E}}}(n_{z,\mathrm{E}} + g\cos\gamma_{\mathrm{E}}) \\ \overline{V}_{\mathrm{E}}\sin\gamma_{\mathrm{E}} \\ \overline{V}_{\mathrm{E}}\cos\gamma_{\mathrm{E}} \end{bmatrix}, \tag{26}$$

$$R = \bar{h}(\bar{x}) \triangleq 1000\sqrt{(\bar{h}_{\mathrm{E}} - \bar{h}_{\mathrm{P}})^2 + (\bar{d}_{\mathrm{E}} - \bar{d}_{\mathrm{P}})^2}. \tag{27}$$

III. Model Predictive Guidance

We implement MPG at the fixed sample rate T_{s} s/step. We assume that measurements of the state and applied control are sampled at each update of the guidance algorithm and are given by

$$x_k \triangleq \bar{x}(kT_{\mathrm{s}}), \quad u_k \triangleq u(kT_{\mathrm{s}}), \tag{28}$$

respectively. At step k, MPG uses the data x_k and u_k at step k to compute the next control u_{k+1}. We define

$$n_{z,\mathrm{E},k} \triangleq n_{z,\mathrm{E}}(kT_{\mathrm{s}}), \quad n_{z,\mathrm{P},k} \triangleq n_{z,\mathrm{P}}(kT_{\mathrm{s}}). \tag{29}$$

A. Prediction of Dynamics

We assume that the estimated time-to-go is equal to $\ell t_{\mathrm{s},k}$, where $\ell \in \mathbb{Z}_+$ is the prediction horizon length and $t_{\mathrm{s},k} \in \mathbb{R}_+$ is the estimated time-to-go sample time at step k. That is, the dynamics (24), (25), are discretized at a sample time of $t_{\mathrm{s},k}$. We implement MPG using a fixed value of ℓ, while $t_{\mathrm{s},k}$ is computed at each iteration to serve as a surrogate for the time-to-go at step k. Figure 2 illustrates this setup where the estimated time-to-go $\ell t_{\mathrm{s},k}$ may vary while the prediction horizon length is constant. We assume that the control is constant over each interval of length ℓ over the prediction horizon. The motivation for this construction are two-fold:

1) Fixed complexity: Since one of the key factors that determines the complexity of a model-predictive algorithm is the prediction horizon length ℓ, fixing it prevents the algorithm from having variable execution time. Therefore, the guidance hardware can be specified based on the fixed complexity of the algorithm and the guidance algorithm utilizes all of the capacity of the hardware at all steps.
2) Efficient variation of discretization step size: As the separation between the pursuer and evader reduces, the estimated time-to-go $\ell t_{\mathrm{s},k}$ reduces, which implies that $t_{\mathrm{s},k}$ reduces. That is, as the pursuer gets closer to the evader, the engagement dynamics are discretized over a smaller sample time $t_{\mathrm{s},k}$, and thus more accurately represent the continuous time dynamics. Heuristically, this means that MPG makes increasingly accurate computations as the separation between the pursuer and evader gets smaller.

Since MPG updates every T_{s} s, the current time is given by kT_{s} where $k \in \mathbb{Z}_+$ is the number of steps that the guidance algorithm has run, and thus, the total estimated engagement time is given by $kT_{\mathrm{s}} + \ell t_{\mathrm{s},k}$. We define the estimated state at time $kT_{\mathrm{s}} + (j+1)t_{\mathrm{s},k}$, for all $j = 0, \ldots, \ell - 1$ as

$$x_{j+1|k} \triangleq x_{j|k} + \tfrac{1}{6}t_{\mathrm{s},k}(k_1 + 4k_3 + k_3) \in \mathbb{R}^8, \tag{30}$$

$$x_{0|k} \triangleq \bar{x}_k \in \mathbb{R}^8, \quad u_{0|k} \triangleq u_k \in \mathbb{R} \tag{31}$$

$$k_1 \triangleq \bar{f}(x_{j|k}, u_{j|k}, -g\cos\gamma_{\mathrm{E}}, kT_{\mathrm{s}} + jt_{\mathrm{s},k}) \in \mathbb{R}^8, \tag{32}$$

$$k_2 \triangleq \bar{f}(x_{j|k} + \tfrac{1}{2}, u_{j|k}, -g\cos\gamma_{\mathrm{E}}, kT_{\mathrm{s}} + (j+\tfrac{1}{2})t_{\mathrm{s},k}) \in \mathbb{R}^8, \tag{33}$$

$$k_3 \triangleq \bar{f}(x_{j|k} + 2k_2 - k_1, u_{j|k}, -g\cos\gamma_{\mathrm{E}}, kT_{\mathrm{s}} + (j+1)t_{\mathrm{s},k}) \in \mathbb{R}^8, \tag{34}$$

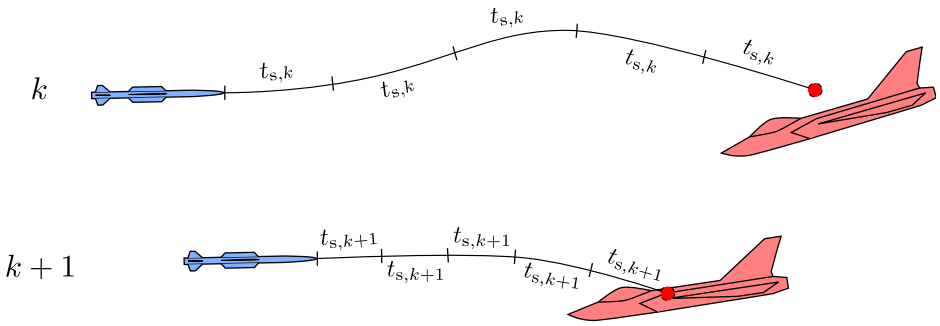

Fig. 2 Fixed-ℓ, varying-$t_{s,k}$ prediction horizon. The prediction horizon length is fixed at $\ell \equiv 5$ and the estimated time-to-go sample time $t_{s,k}$ varies with k. Note that in the illustrated scenario $t_{s,k+1} < t_{s,k}$.

where $u_{j|k} \in \mathbb{R}$ is constant over the interval $[kT_s + jt_{s,k}, kT_s + (j+1)t_{s,k}]$. Note that (30)–(34) represents the integration of the engagement dynamics (24), from the current time kT_s to the estimated end-of-engagement time $kT_s + \ell t_{s,k}$, using a third-order Runge-Kutta method with the assumption that the evader's flight-path angle γ_E is constant. Note that setting $n_{z,E} = -g\cos\gamma_E$ in (13) yields $\dot{\gamma}_E = 0$.

Next, define the estimated terminal range in km

$$R_{\ell|k} \triangleq \bar{h}(x_{\ell|k}). \tag{35}$$

Note that using (30)–(34), $\bar{x}_{\ell|k}$ and $R_{\ell|k}$ can be computed given the measurement $\bar{x}_k$, the last applied control u_k, MPG step k, the estimated time-to-go sample time $t_{s,k}$, and the future control sequence $U_k \triangleq \begin{bmatrix} u_{1|k} & \dots & u_{\ell-1|k} \end{bmatrix}^T \in \mathbb{R}^{\ell-1}$. We express this relationship as

$$f_R(U_k, x_k, u_k, k, t_{s,k}) \colon \mathbb{R}^{\ell-1} \times \mathbb{R}^8 \times \mathbb{R} \times \mathbb{Z}_+ \times \mathbb{R}_+ \to \mathbb{R}_+, \tag{36}$$

where f_R is a function that computes the value of $R_{\ell,k}$ using U, x_k, u_k, k, and t_s, and U is the future sequence of controls that is to be computed using MPG.

B. Guidance Law Update Using Optimization

We define the the numerically computed gradient of (36) with respect to U as

$$\nabla R_{\ell|k}(U, t_s) \triangleq \begin{bmatrix} \nabla R_{\ell|k,1}(U, t_s) & \cdots & \nabla R_{\ell|k,\ell-1}(U, t_s) \end{bmatrix} \in \mathbb{R}^{1\times(\ell-1)}, \tag{37}$$

where

$$\nabla R_{\ell|k,i}(U, t_s) \triangleq \frac{f_R(U + e_i\varepsilon, x_k, u_k, k, t_s) - f_R(U, x_k, u_k, k, t_s)}{\varepsilon} \in \mathbb{R}, \tag{38}$$

for all $i = 1, \dots, \ell - 1$, $e_i \in \mathbb{R}^{\ell-1}$ is the i-th standard basis vector, and $\varepsilon = 10^{-6}$.

The following algorithm is used to set the value of the initial estimated time-to-go sample time $t_{s,0}$.

$t_{s,0}$ Initialization Algorithm

For $j = 0, \dots, \text{floor}(50/T_s)$, we compute $x_{j+1|k}$ using (30) with $x_{0|0} = \bar{x}_0$, $k = 0$, $u_{j|k} \equiv 0$, and $t_{s,k} = T_s$. Next, we compute

$$R_{j+1|k} = \bar{h}(x_{j+1|k}), \tag{39}$$

and define $j_{\min}$ to be the value of j for which $R_{j+1|k}$ is smallest. Finally, we define

$$t_{s,0} \triangleq \frac{j_{\min} T_s}{\ell}. \tag{40}$$

That is, we simulate the engagement dynamics under no control to compute the first estimate of the time-to-go $t_{s,0}$ as the time at which the separation between the pursuer and evader is smallest.

Since the ability of a missile autopilot to follow normal acceleration commanded is physically imitated, we incorporate constraints on the normal acceleration command $n_{z,P}$ in the optimization algorithm. In particular, we require that the following constraints on the entries of the predicted sequence of controls U_k are enforced

$$|u_{i|k}| \leq u_{\max}, \quad i = 1, \ldots, \ell - 1, \tag{41}$$

$$|u_{1|k} - u_k| \leq \dot{u}_{\max} T_s, \tag{42}$$

$$|u_{i|k} - u_{i-1|k}| \leq \dot{u}_{\max} t_{s,k}, \quad i = 2, \ldots, \ell - 1, \tag{43}$$

where $u_{\max}$ and $\dot{u}_{\max}$ are the maximum allowable normal acceleration magnitude in $\mathrm{m/s^2}$ and maximum allowable normal acceleration rate magnitude in $\mathrm{m/s^3}$. Note that that desired normal acceleration rate constraints are specified as (42), (43), since in general $t_{s,k} \neq T_s$, and $u_{1|k}$, which is the next control, is required to satisfy the rate constraint (42) at each iteration of MPG.

Define

$$\theta_N \triangleq \mathrm{GDC}(\theta_0, t_s, T_s, N, u_{\max}, \dot{u}_{\max}), \tag{44}$$

where $\mathrm{GDC}(\theta_0, t_s, T_s, N, u_{\max}, \dot{u}_{\max})$ represents the optimizations algorithm given below, which uses Nesterov's accelerated gradient descent [24, p. 76] with constrained step and momentum sizes. Given

$$\theta_0 = \tilde{\theta}_0 = \begin{bmatrix} \theta_{1,0} & \cdots & \theta_{\ell-1,0} \end{bmatrix}^{\mathrm{T}} \in \mathbb{R}^{\ell-1}$$

and $t_s \in \mathbb{R}_+$, for $i = 0, \ldots, N - 1$, we compute

$$\theta_{i+1} \triangleq \begin{cases} \tilde{\theta}_i - \gamma_i \nabla R_{\ell|k}(\tilde{\theta}_i, t_s), & \nabla R_{\ell|k}(\tilde{\theta}_i, t_s) \neq 0, \\ \tilde{\theta}_i, & \nabla R_{\ell|k}(\tilde{\theta}_i, t_s) = 0, \end{cases} \tag{45}$$

$$\tilde{\theta}_{i+1} \triangleq \theta_{i+1} + \mu_i(\theta_{i+1} - \theta_i), \tag{46}$$

where θ_i and $\tilde{\theta}_i$ are the optimization and intermediate variables of the form $\theta_i = \begin{bmatrix} \theta_{1,i} & \cdots & \theta_{\ell-1,i} \end{bmatrix}^{\mathrm{T}} \in \mathbb{R}^{\ell-1}$ and $\tilde{\theta}_i = \begin{bmatrix} \tilde{\theta}_{1,i} & \cdots & \tilde{\theta}_{\ell-1,i} \end{bmatrix}^{\mathrm{T}} \in \mathbb{R}^{\ell-1}$, respectively, and $\gamma_i \in \mathbb{R}_+$ is the gradient-descent step size given by

$$\gamma_i \triangleq \begin{cases} \frac{1}{\|\nabla R_{\ell|k}(\tilde{\theta}_i, t_s)\|}, & \frac{1}{\|\nabla R_{\ell|k}(\tilde{\theta}_i, t_s)\|} \leq \gamma_{\max,i} \\ \gamma_{\max,i}, & \text{otherwise}, \end{cases} \tag{47}$$

where

$$\gamma_{\max,i} \triangleq \min \begin{bmatrix} \gamma_{\mathrm{rate},i} \\ \gamma_{\mathrm{mag},i} \end{bmatrix}, \quad \gamma_{\mathrm{rate},i} \triangleq \begin{bmatrix} \gamma_{\mathrm{rate},1,i} \\ \vdots \\ \gamma_{\mathrm{rate},\ell-1,i} \end{bmatrix}, \quad \gamma_{\mathrm{mag},i} \triangleq \begin{bmatrix} \gamma_{\mathrm{mag},1,i} \\ \vdots \\ \gamma_{\mathrm{mag},\ell-1,i} \end{bmatrix}, \tag{48}$$

$$\gamma_{\mathrm{rate},1,i} \triangleq \begin{cases} (\tilde{\theta}_{1,i} - \theta_{1,0} + \dot{u}_{\max} T_s)/\nabla R_{\ell|k,1}(\tilde{\theta}_i, t_s), & \nabla R_{\ell|k,1}(\tilde{\theta}_i, t_s) > 0, \\ (\tilde{\theta}_{1,i} - \theta_{1,0} - \dot{u}_{\max} T_s)/\nabla R_{\ell|k,1}(\tilde{\theta}_i, t_s), & \nabla R_{\ell|k,1}(\tilde{\theta}_i, t_s) < 0, \\ 0, & \nabla R_{\ell|k,1}(\tilde{\theta}_i, t_s) = 0, \end{cases} \tag{49}$$

for all $j = 2, \ldots, \ell - 1$,

$$\gamma_{\mathrm{rate},j,i} \triangleq \begin{cases} (\tilde{\theta}_{j,i} - \theta_{j,0} + \dot{u}_{\max} t_s)/\nabla R_{\ell|k,j}(\tilde{\theta}_i, t_s), & \nabla R_{\ell|k,j}(\tilde{\theta}_i, t_s) > 0, \\ (\tilde{\theta}_{j,i} - \theta_{j,0} - \dot{u}_{\max} t_s)/\nabla R_{\ell|k,j}(\tilde{\theta}_i, t_s), & \nabla R_{\ell|k,j}(\tilde{\theta}_i, t_s) < 0, \\ 0, & \nabla R_{\ell|k,j}(\tilde{\theta}_i, t_s) = 0, \end{cases} \tag{50}$$

for all $j = 1, \ldots, \ell - 1$,

$$\gamma_{\mathrm{mag},j,i} \triangleq \begin{cases} (\tilde{\theta}_{j,i} + u_{\max})/\nabla R_{\ell|k,j}(\tilde{\theta}_i, t_\mathrm{s}), & \nabla R_{\ell|k,j}(\tilde{\theta}_i, t_\mathrm{s}) > 0, \\ (\tilde{\theta}_{j,i} - u_{\max})/\nabla R_{\ell|k,j}(\tilde{\theta}_i, t_\mathrm{s}), & \nabla R_{\ell|k,j}(\tilde{\theta}_i, t_\mathrm{s}) < 0, \\ 0, & \nabla R_{\ell|k,j}(\tilde{\theta}_i, t_\mathrm{s}) = 0, \end{cases} \tag{51}$$

$\mu_i \in \mathbb{R}_+$ is the momentum parameter given by

$$\mu_i \triangleq \max(1, \mu_{\max,i}), \tag{52}$$

where

$$\mu_{\max,i} \triangleq \min \begin{bmatrix} \mu_{\mathrm{rate},i} \\ \mu_{\mathrm{mag},i} \end{bmatrix}, \quad \mu_{\mathrm{rate},i} \triangleq \begin{bmatrix} \mu_{\mathrm{rate},1,i} \\ \vdots \\ \mu_{\mathrm{rate},\ell-1,i} \end{bmatrix}, \quad \mu_{\mathrm{mag},i} \triangleq \begin{bmatrix} \mu_{\mathrm{mag},1,i} \\ \vdots \\ \mu_{\mathrm{mag},\ell-1,i} \end{bmatrix}, \tag{53}$$

$$\mu_{\mathrm{rate},1,i} \triangleq \begin{cases} \theta_{1,0} + \dot{u}_{\max} T_\mathrm{s} - \theta_{1,i}, & \theta_{i+1,1} - \theta_{i,1} > 0, \\ \theta_{1,0} - \dot{u}_{\max} T_\mathrm{s} - \theta_{1,i}, & \theta_{i+1,1} - \theta_{i,1} < 0, \\ 0, & \theta_{i+1} - \theta_i = 0, \end{cases} \tag{54}$$

for all $j = 2, \ldots, \ell - 1$,

$$\mu_{\mathrm{rate},j,i} \triangleq \begin{cases} \theta_{j,0} + \dot{u}_{\max} T_\mathrm{s} - \theta_{j,i}, & \theta_{i+1,1} - \theta_{i,1} > 0, \\ \theta_{j,0} - \dot{u}_{\max} T_\mathrm{s} - \theta_{j,i}, & \theta_{i+1,1} - \theta_{i,1} < 0, \\ 0, & \theta_{i+1,1} - \theta_{i,1} = 0, \end{cases} \tag{55}$$

and for all $j = 1, \ldots, \ell - 1$,

$$\mu_{\mathrm{mag},j,i} \triangleq \begin{cases} u_{\max} - \theta_{j,i}, & \theta_{i+1,1} - \theta_{i,1} > 0, \\ -u_{\max} - \theta_{j,i}, & \theta_{i+1,1} - \theta_{i,1} < 0, \\ 0, & \theta_{i+1,1} - \theta_{i,1} = 0. \end{cases} \tag{56}$$

Note that the constrained gradient descent algorithm (44) enforces the constraints (41)–(43) on the minimizer by limiting the gradient-descent step size and the momentum parameter. Furthermore, t_s is constant in the algorithm.

At each step k we define

$$\underline{t}_{\mathrm{s},k} \triangleq 0.99 t_{\mathrm{s},k}, \quad \overline{t}_{\mathrm{s},k} \triangleq 1.01 t_{\mathrm{s},k}. \tag{57}$$

and compute

$$\underline{U}_{\mathrm{opt},k} \triangleq \mathrm{GDC}(U_k, \underline{t}_{\mathrm{s},k}, T_\mathrm{s}, N, u_{\max}, \dot{u}_{\max}), \tag{58}$$

$$U_{\mathrm{opt},k} \triangleq \mathrm{GDC}(U_k, t_{\mathrm{s},k}, T_\mathrm{s}, N, u_{\max}, \dot{u}_{\max}), \tag{59}$$

$$\overline{U}_{\mathrm{opt},k} \triangleq \mathrm{GDC}(U_k, \overline{t}_{\mathrm{s},k}, T_\mathrm{s}, N, u_{\max}, \dot{u}_{\max}). \tag{60}$$

Next, we define the updated sequence of controls U_{k+1} and the next estimated time-to-go sample time $t_{\mathrm{s},k+1}$ as

$$\{U_{k+1}, \tilde{t}_{\mathrm{s},k+1}\} \triangleq \operatorname{argmin} f_R(U, x_k, u_k, k, t_\mathrm{s}), \quad \{U, t_\mathrm{s}\} \in \{\{\underline{U}_{\mathrm{opt}}, \underline{t}_{\mathrm{s},k}\}, \{U_{\mathrm{opt}}, t_{\mathrm{s},k}\}, \{\overline{U}_{\mathrm{opt}}, \overline{t}_{\mathrm{s},k}\}\}, \tag{61}$$

$$t_{\mathrm{s},k+1} \triangleq \tilde{t}_{\mathrm{s},k+1} - \frac{T_\mathrm{s}}{\ell}. \tag{62}$$

Note that (62) accounts for the passing of T_s s by the time the next iteration of MPG starts. Finally, we define

$$n_{z,\mathrm{P},k} = u_{k+1} \triangleq u_{1|k+1}. \tag{63}$$

C. Pursuer and Evader Models

We model the pursuer as a beyond-visual-range (BVR) air-to-air missile. For simplicity we assume that pursuer has a constant mass $m_{\mathrm{P}} = 130$ kg. The pursuer thrust T_{P} is given by

$$T_{\mathrm{P}}(t) = \begin{cases} 11,000 \text{ N}, & 0 \text{ s} \leq t < 10 \text{ s}, \\ 1,800 \text{ N}, & 10 \text{ s} \leq t < 30 \text{ s}, \\ 0 \text{ N}, & t > 30 \text{ s}, \end{cases} \tag{64}$$

which models a boost-sustain rocket motor. Note that (64) is the source of the explicit time dependence of the dynamics (24). The drag coefficient of the pursuer $C_{\mathrm{d,P}}(\mathrm{M_P})$ is given by

$$C_{\mathrm{d,P}}(\mathrm{M_P}) = \frac{0.01532\mathrm{M_P^4} - 0.03587\mathrm{M_P^3} + 0.08588\mathrm{M_P^2} - 0.1047\mathrm{M_P} + 0.04269}{\mathrm{M_P^4} - 3.394\mathrm{M_P^3} + 6.806\mathrm{M_P^2} - 7.011\mathrm{M_P} + 2.672}. \tag{65}$$

$S_{\mathrm{P}} = 2.3$ m is the reference surface area of the pursuer. Figure 3(a) shows $C_{\mathrm{d,P}}(\mathrm{M_P})$ versus $\mathrm{M_P}$.

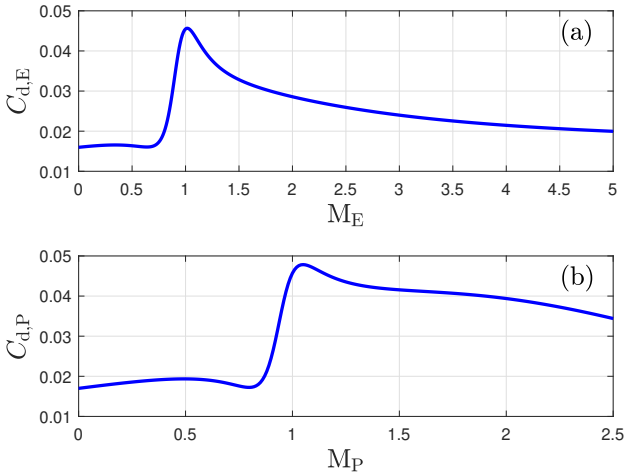

Fig. 3 (a) shows $C_{\mathrm{d,P}}(\mathrm{M_P})$ versus $\mathrm{M_P}$ and (b) shows $C_{\mathrm{d,E}}(\mathrm{M_E})$ versus $\mathrm{M_E}$.

We model the evader as a medium-weight fighter jet. For simplicity we assume that the evader has a constant mass $m_{\mathrm{E}} = 10000$ kg. We assume that the evader fighter-jet is at maximum military power given by

$$T_{\mathrm{P}}(h_{\mathrm{E}}) = \frac{\rho(h_{\mathrm{E}})}{\rho(0)} 76310 \text{ N}, \tag{66}$$

which is an approximation [25, p. 176] of the maximum dry thrust at the altitude h_{E} for a turbofan engine that produces 76310 N at sea level. The drag coefficient of the evader $C_{\mathrm{d,E}}(\mathrm{M_E})$ is given by

$$C_{\mathrm{d,E}}(\mathrm{M_E}) = \frac{0.1342\mathrm{M_E^2} - 0.239\mathrm{M_E} + 0.108}{\mathrm{M_E^4} - 5.545\mathrm{M_E^3} + 14.86\mathrm{M_E^2} - 16.6\mathrm{M_E} + 6.355}. \tag{67}$$

$S_{\mathrm{E}} = 28$ m is the reference surface area of the evader. In practice a functional representation of the drag coefficients (65), (67) can be obtained by curve-fitting. Figure 3(b) shows $C_{\mathrm{d,E}}(\mathrm{M_E})$ versus $\mathrm{M_E}$.

IV. Augmented Proportional Guidance

We simulate the augmented proportional guidance (APG) law to serve as a baseline performance metric. In particular, we implement the APG law given in [1, p. 166] modified to be discrete-time and with gravity correction as

$$n_{z,\mathrm{P},k} = u_{k+1} = 3\dot{R}_k\dot{\beta}_k + \frac{3}{2}(n_{z,\mathrm{E},k} + g\cos\gamma_{\mathrm{E},k}) - g\cos\gamma_{\mathrm{P},k}, \tag{68}$$

where the sampled range-rate in m/s is given by

$$\dot{R}_k = \frac{(\bar{h}_{\mathrm{E},k} - \bar{h}_{\mathrm{P},k})(\overline{V}_{\mathrm{E},k} \sin\gamma_{\mathrm{E},k} - \overline{V}_{\mathrm{P},k} \sin\gamma_{\mathrm{P},k}) + (\bar{d}_{\mathrm{E}} - \bar{d}_{\mathrm{P}})(\overline{V}_{\mathrm{E},k} \cos\gamma_{\mathrm{E},k} - \overline{V}_{\mathrm{P},k} \cos\gamma_{\mathrm{P},k})}{\sqrt{(\bar{h}_{\mathrm{E},k} - \bar{h}_{\mathrm{P},k})^2 + (\bar{d}_{\mathrm{E},k} - \bar{d}_{\mathrm{P},k})^2}} 1000, \tag{69}$$

and the sampled line-of-sight-angle rate is given by

$$\dot{\beta}_k = \frac{(\bar{d}_{\mathrm{E},k} - \bar{d}_{\mathrm{P},k})(\overline{V}_{\mathrm{E},k} \sin\gamma_{\mathrm{E},k} - \overline{V}_{\mathrm{P},k} \sin\gamma_{\mathrm{P},k}) - (\bar{h}_{\mathrm{E},k} - \bar{h}_{\mathrm{P},k})(\overline{V}_{\mathrm{E},k} \cos\gamma_{\mathrm{E},k} - \overline{V}_{\mathrm{P},k} \cos\gamma_{\mathrm{P},k})}{(\bar{d}_{\mathrm{E},k} - \bar{d}_{\mathrm{P},k})^2 + (\bar{h}_{\mathrm{E},k} - \bar{h}_{\mathrm{P},k})^2}, \tag{70}$$

where the sampled line-of-sight angle is defined by

$$\beta_k \triangleq \theta_{\vec{r}_{\mathrm{E/P}}/\hat{\imath}_{\mathrm{A}}/\hat{\jmath}_{\mathrm{A}}} = \operatorname{atan2}(\bar{h}_{\mathrm{E},k} - \bar{h}_{\mathrm{P},k}, \bar{d}_{\mathrm{E},k} - \bar{d}_{\mathrm{P},k}), \tag{71}$$

and

$$\overline{V}_{\mathrm{P},k} \triangleq \overline{V}_{\mathrm{P}}(kT_{\mathrm{s}}), \quad \gamma_{\mathrm{P},k} \triangleq \gamma_{\mathrm{P}}(kT_{\mathrm{s}}), \quad \bar{h}_{\mathrm{P},k} \triangleq \bar{h}_{\mathrm{P}}(kT_{\mathrm{s}}), \quad \bar{d}_{\mathrm{P},k} \triangleq \bar{d}_{\mathrm{P}}(kT_{\mathrm{s}}), \tag{72}$$

$$\overline{V}_{\mathrm{E},k} \triangleq \overline{V}_{\mathrm{E}}(kT_{\mathrm{s}}), \quad \gamma_{\mathrm{E},k} \triangleq \gamma_{\mathrm{E}}(kT_{\mathrm{s}}), \quad \bar{h}_{\mathrm{E},k} \triangleq \bar{h}_{\mathrm{E}}(kT_{\mathrm{s}}), \quad \bar{d}_{\mathrm{E},k} \triangleq \bar{d}_{\mathrm{E}}(kT_{\mathrm{s}}). \tag{73}$$

Note that implementation of APG (68) requires knowledge of the normal acceleration of the evader $n_{z,\mathrm{E},k}$, which is not required by MPG.

V. Examples

We simulate the engagement dynamics (24) discretized at T_{s} s, where the intersample dynamics are simulated using MATLAB's ode45 function. We define the miss distance as the distance of closest approach and a miss distance of less than 10 m is considered a successful intercept. For all of the examples, for MPG unless stated otherwise we set $T_{\mathrm{s}} = 0.1$ s, $\ell = 10$, $N = 20$, $u_{\max} = 40\mathrm{g}$, and $\dot{u}_{\max} = 4\mathrm{g}$, where $g = 9.81$ m/s^2.

Example 1. *Tail Chase, Nonmaneuvering Evader.* Let

$$\overline{V}_{\mathrm{P},0} = 0.45 \text{ km}, \quad \gamma_{\mathrm{P},0} = 0 \text{ rad}, \quad \bar{h}_{\mathrm{P},0} = 13 \text{ km}, \quad \bar{d}_{\mathrm{P},0} = 0 \text{ km}, \tag{74}$$

$$\overline{V}_{\mathrm{E},0} = 0.45 \text{ km}, \quad \gamma_{\mathrm{E},0} = 0 \text{ rad}, \quad \bar{h}_{\mathrm{E},0} = 13 \text{ km}, \quad \bar{d}_{\mathrm{E},0} = 8 \text{ km}, \tag{75}$$

$$n_{z,\mathrm{E},k} = -g \cos\gamma_{\mathrm{E},k}. \tag{76}$$

We simulate the engagement specified by (74)–(76) using MPG and APG. Figure 4 shows the trajectory followed by the pursuer using MPG. The trajectory followed by the pursuer with APG is not shown since for this example it represents a nonmaneuvering tail-chase trajectory. The APG time-of-flight and terminal value of $\dot{R}_k$ are used to compute the time and closing speed advantage achieved by MPG over APG. The pursuer using MPG intercepts the evader with a time advantage of 1.27 s and a closing-speed advantage of 42 m/s. Figure 5 shows the commanded normal acceleration $n_{z,\mathrm{P},k}$ versus time.

Next, we simulate the engagement specified by (74)–(76) with various choices of $d_{\mathrm{E},0}$ using MPG and APG. Figure 6 plots the time and closing-speed advantage achieved by MPG over APG versus $d_{\mathrm{E},0}$. ◇

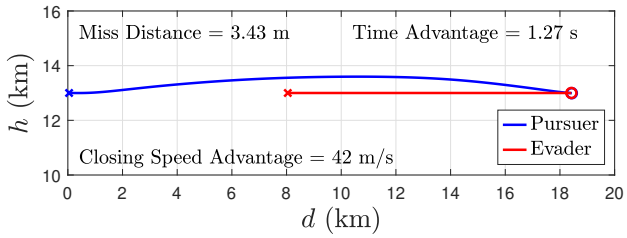

Fig. 4 Example 1: Pursuer and evader trajectories.

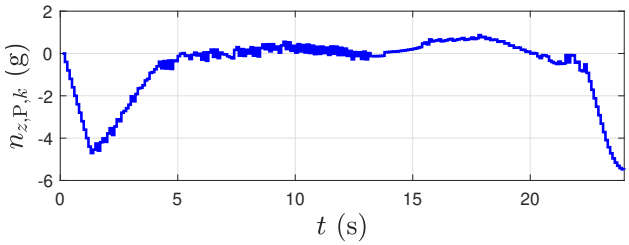

Fig. 5 Example 1: Pursuer commanded normal acceleration.

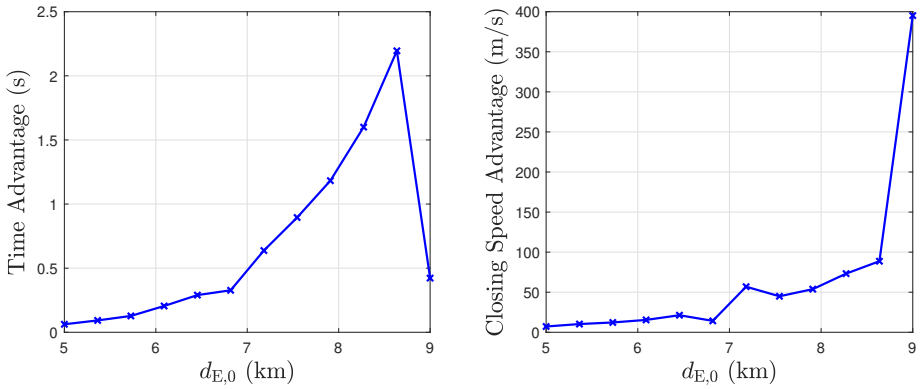

Fig. 6 Example 1: Time and closing-speed advantage achieved by MPG relative to APG.

Example 2. *Tail Chase, Maneuvering Evader.* Let the initial condition of the engagement be given by (74) and (75), and the evader normal acceleration be given by

$$n_{z,\mathrm{E},k} = -g\cos\gamma_{\mathrm{E},k} + 7\cos 0.01k. \tag{77}$$

We simulate the engagement using MPG and APG. Figure 7(a) and Figure 7(c) shows the trajectories followed by the pursuer and evader using MPG and APG, respectively. Figure 7(b) and Figure 7(b) shows the pursuer commanded normal acceleration using MPG and APG, respectively. The pursuer using MPG intercepts the evader with a time advantage of 1.87 s and a closing-speed advantage of 62 m/s.

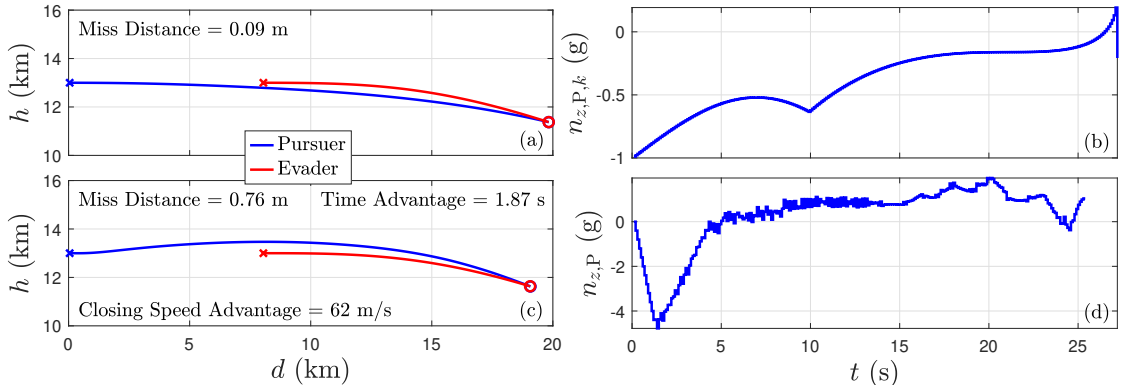

Fig. 7 Example 2: For a maneuvering evader (a) and (b) show the pursuer-evader trajectories and the pursuer commanded normal acceleration using APG, respectively; (c) and (d) show the pursuer-evader trajectories and the pursuer commanded normal acceleration using MPG, respectively. The pursuer with MPG intercepts the evader with a time and closing-speed advantage of 1.87 **s and** 62 **m/s, respectively.**

Next, we repeat the above example with $\bar{d}_{\mathrm{E},0} = 9$ km. Figure 8 shows that pursuer with APG is not able to intercept

the evader, whereas the pursuer with MPG intercepts the evader with a miss distance of 0.21 m.

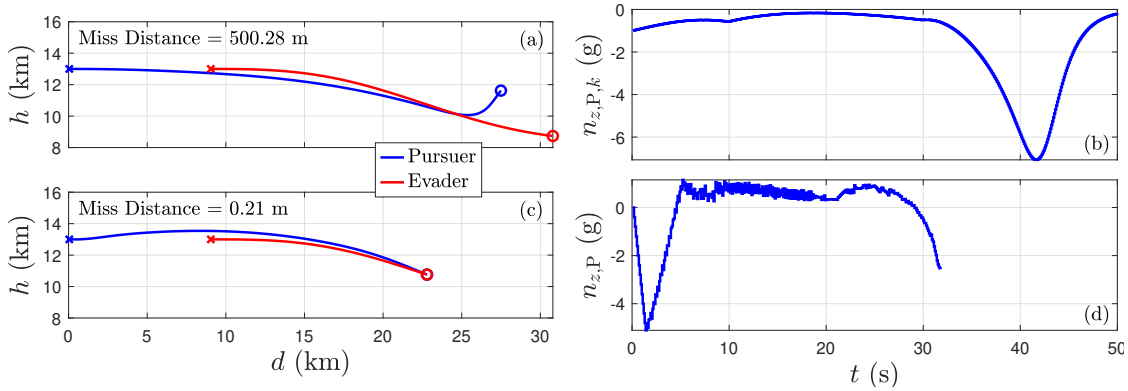

Fig. 8 Example 2: For a maneuvering evader (a) and (b) show the pursuer-evader trajectories and the pursuer commanded normal acceleration using APG, respectively; (c) and (d) show the pursuer-evader trajectories and the pursuer commanded normal acceleration using MPG, respectively. The pursuer with APG fails to intercept the evader.

Next, we simulate the engagement dynamics with the initial condition of the engagement given by (74) and (75) with $\bar{d}_{\mathrm{E},0} = 7$ km, and the evader normal acceleration given by

$$n_{z,\mathrm{E},k} = -g\cos\gamma_{\mathrm{E},k} + 7\cos 0.06k. \tag{78}$$

Figure 9 shows that the pursuer with MPG fails to intercept the evader. Figure 10(a) shows the time-to-go for the pursuer

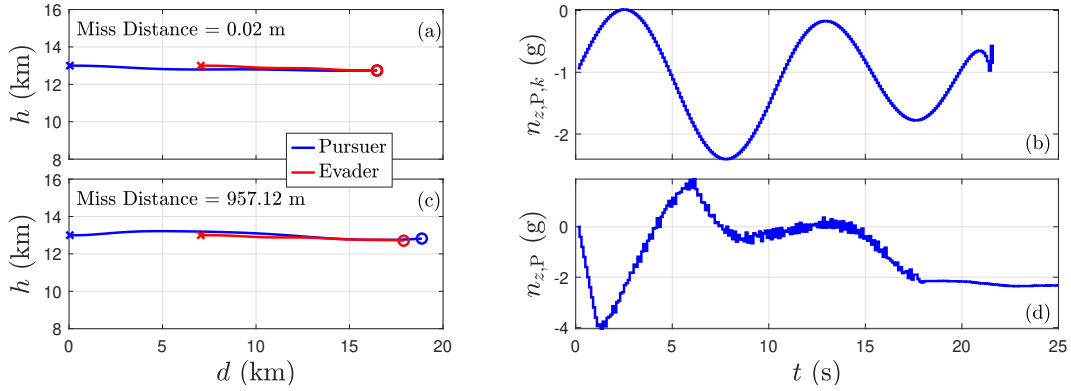

Fig. 9 Example 2: For a maneuvering evader (a) and (b) show the pursuer-evader trajectories and the pursuer commanded normal acceleration using APG, respectively; (c) and (d) show the pursuer-evader trajectories and the pursuer commanded normal acceleration using MPG, respectively. The pursuer with MPG fails to intercept the evader.

with APG and the estimated time-to-go for the pursuer with MPG. We compute the time-to-go for the pursuer with APG after the completion of the engagement simulation. Note that the estimate time-to-go for the pursuer with MPG is given by $\ell t_{\mathrm{s},k}$. Figure 10(b) shows the estimated terminal range $R_{\ell|k}$. Figure 10 suggests that MPG fails due to poor estimates of time-to-go and terminal range. Finally, we repeat the previous engagement simulation with $\ell = 20$. Figure 11 shows that both pursuers intercept the evader. This simulation suggests that MPG may be less robust than APG depending on the choice of tuning parameters. However, increasing ℓ or N to increase MPG's robustness will incur a penalty in computational complexity. Figure 12 shows the estimated time-to-go and estimated terminal range for the pursuer with MPG. ◇

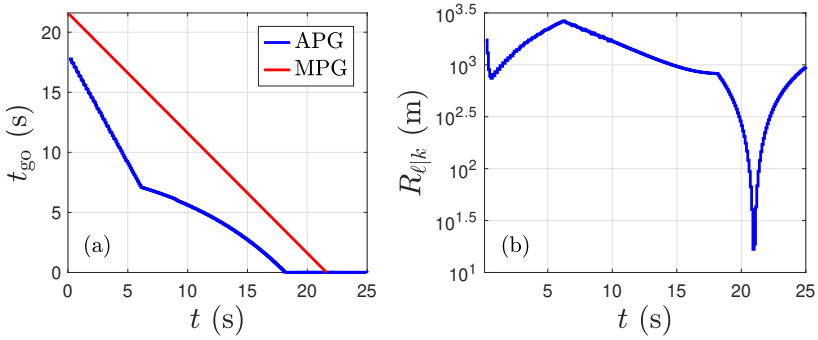

Fig. 10 Example 2: For a maneuvering evader (a) shows the time-to-go for the pursuer with APG and the estimated time-to-go for the pursuer with MPG, and (b) shows the estimated terminal range $R_{\ell|k}$ estimated by MPG.

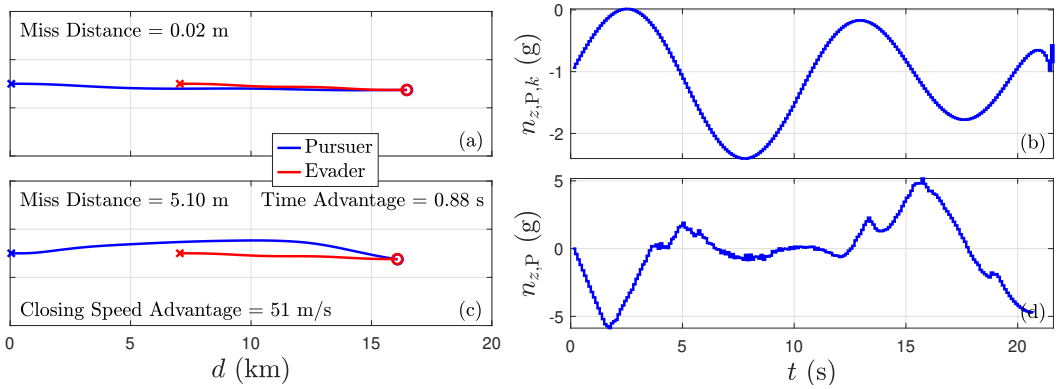

Fig. 11 Example 2: For a maneuvering evader (a) and (b) show the pursuer-evader trajectories and the pursuer commanded normal acceleration using APG, respectively; (c) and (d) show the pursuer-evader trajectories and the pursuer commanded normal acceleration using MPG, respectively. The pursuer with MPG achieves a time and closing-speed advantage of 0.88 s and 51 m/s, respectively.

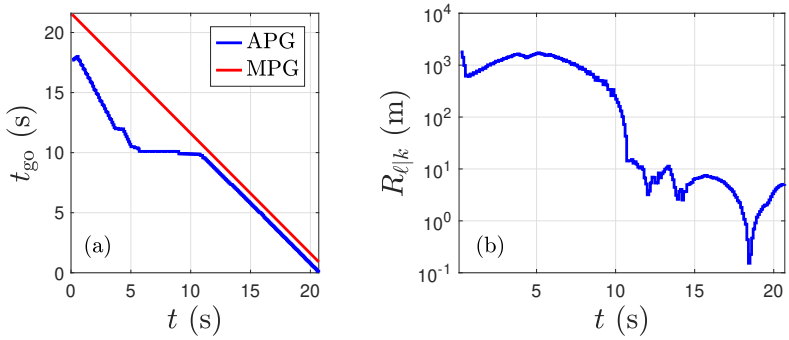

Fig. 12 Example 2: For a maneuvering evader (a) shows the time-to-go for the pursuer with APG and the estimated time-to-go for the pursuer with MPG, and (b) shows the estimated terminal range $R_{\ell|k}$ estimated by MPG.

Example 3. *Headon, Nonmaneuvering Target.* Let the pursuer initial conditions be given by (74) and let

$$\bar{V}_{\mathrm{E},0} = 0.45 \text{ km}, \quad \gamma_{\mathrm{E},0} = \pi \text{ rad}, \quad \bar{h}_{\mathrm{E},0} = 18 \text{ km}, \quad \bar{d}_{\mathrm{E},0} = 35 \text{ km}, \tag{79}$$

$$n_{z,\mathrm{E},k} = -g \cos \gamma_{\mathrm{E},k} - 6 \sin 0.01k. \tag{80}$$

We simulate the engagement using MPG and APG. Figure 13(a) and Figure 13(c) shows the trajectories followed by the pursuer and evader using MPG and APG, respectively. Figure 13(b) and Figure 13(b) shows the pursuer commanded normal acceleration using MPG and APG, respectively. The pursuer using MPG intercepts the evader with a time advantage of 0.20 s and a closing-speed advantage of 33 m/s. ◇

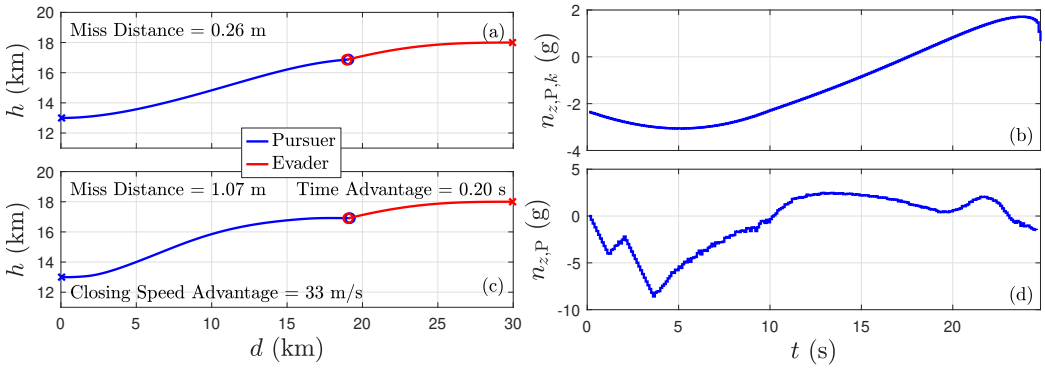

Fig. 13 Example 3: For a maneuvering evader (a) and (b) show the pursuer-evader trajectories and the pursuer commanded normal acceleration using APG, respectively; (c) and (d) show the pursuer-evader trajectories and the pursuer commanded normal acceleration using MPG, respectively. The pursuer with MPG achieves a time and closing-speed advantage of 0.20 **s and** 33 **m/s, respectively.**

Example 4. *Anti-Missile Defense Engagement.* Let

$$\overline{V}_{\mathrm{P},0} = 0.1 \text{ km}, \quad \gamma_{\mathrm{P},0} = \tfrac{1}{2}\pi \text{ rad}, \quad \bar{h}_{\mathrm{P},0} = 0 \text{ km}, \quad \bar{d}_{\mathrm{P},0} = 0 \text{ km}, \tag{81}$$

$$\overline{V}_{\mathrm{E},0} = 0.1 \text{ km}, \quad \gamma_{\mathrm{E},0} = \frac{21}{20}\pi \text{ rad}, \quad \bar{h}_{\mathrm{E},0} = 4 \text{ km}, \quad \bar{d}_{\mathrm{E},0} = 10 \text{ km}, \tag{82}$$

$$n_{z,\mathrm{E},k} = -g\cos\gamma_{\mathrm{E},k} - 30\sin 0.06k, \tag{83}$$

which represents an engagement scenario where the pursuer is launched vertically from sea level to intercept in incoming pursuer. For this example, we simulate the interception of a missile evader using a missile pursuer. In particular, we set

$$m_{\mathrm{E}} = m_{\mathrm{P}}, \quad s_{\mathrm{E}} = s_{\mathrm{P}}, \quad T_{\mathrm{E}} = T_{\mathrm{P}}, \tag{84}$$

which specifies the evader as missile. We simulate the engagement using MPG and APG. Figure 14(a) and Figure 14(c) shows the trajectories followed by the pursuer and evader using MPG and APG, respectively. Figure 14(b) and Figure 14(b) shows the pursuer commanded normal acceleration using MPG and APG, respectively. The pursuer using MPG intercepts the evader, whereas the pursuer using APG is not able to intercept the evader. ◇

VI. Conclusions and Future Work

This article presented a numerical investigation of model predictive guidance (MPG), which uses a nonlinear, scenario-specific engagement model and model-predictive guidance concepts to produce normal acceleration commands for a pursuer. MPG utilizes gradient descent with Nesterov's accelerated gradient descent to solve the optimization at each step of the algorithm. Magnitude and rate constraints on the normal acceleration commands for the pursuer are satisfied by constraining the gradient descent step size at each step. Another feature of MPG was the use of fixed-size, variable-time horizon, which divides the horizon into smaller and smaller steps as the estimated engagement time decreases. This feature facilitates fixed-computational complexity. In order to reduce the engagement time, a heuristic technique was utilized. In particular, at each step the optimization was performed for three choices of estimated engagement time and the minimum-time solution was selected as the solution for that step. Several features of MPG were designed with real-time implementation in mind.

The performance of MPG was investigated to highlight its applicability in diverse scenarios. Augmented proportional guidance (APG) was used as a benchmark for a guidance law that is designed for maneuvering targets. Several numerical

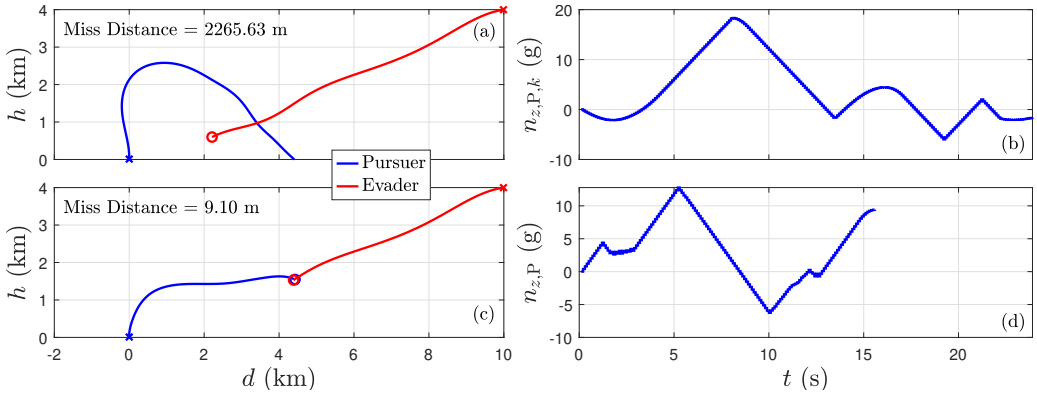

Fig. 14 Example 4: For a maneuvering evader (a) and (b) show the pursuer-evader trajectories and the pursuer commanded normal acceleration using APG, respectively; (c) and (d) show the pursuer-evader trajectories and the pursuer commanded normal acceleration using MPG, respectively. The pursuer with APG is not able to intercept the evader.

examples with missile-on-jet engagements demonstrated that pursuers with MPG intercept evaders in less time compared to pursuers with APG. MPG was also applied to a scenario where a ground-based missile is used to intercept an air-to-ground missile.

The most immediate next step for MPG is its extension from planar engagements to 3D engagements. This modification may be straightforward as only the engagement dynamics will need to be extended without the need for modifying the algorithm. The highest priority for future research is a detailed investigation of the robustness of MPG to sensor noise, engagement scenarios, and tuning parameters. Furthermore, improvement in robustness may be achievable by modifying the optimization scheme. Finally, another next step is the inclusion of an appropriate observer to circumvent the requirement of full-state measurements.

Acknowledgments

This research was supported by ONR under BRC grant N00014-18-1-2211.

References

[1] Zarchan, P., *Tactical and Strategic Missile Guidance*, sixth ed., AIAA, 2012.

[2] Murtaugh, S. A., and Criel, H. E., "Fundamentals of proportional navigation," *IEEE Spectrum*, Vol. 3, No. 12, 1966, pp. 75–85.

[3] Zarchan, P., "Proportional navigation and weaving targets," *AIAA J. Guid. Contr. Dyn.*, Vol. 18, No. 5, 1995, pp. 969–974.

[4] Nesline., F. W., and Zarchan, P., "A New Look at Classical vs Modern Homing Missile Guidance," *AIAA J. Guid. Contr. Dyn.*, Vol. 4, No. 1, 1981, pp. 78–85.

[5] Cheng, V., and Gupta, N., "Advanced Midcourse Guidance for Air-to-Air Missiles," *AIAA J. Guid. Contr. Dyn.*, Vol. 9, No. 2, 1986, pp. 135–142.

[6] Menon, P., and Briggs, M., "A Midcourse Guidance Law for Air-to-Air Missiles," *AIAA Guid. Nav. Contr. Conf. Ex.*, 1987, pp. 1070–1079. A87-50515.

[7] Lin, C., and Tsai, L., "Analytical Solution of Optimal Trajectory-Shaping Guidance," *AIAA J. Guid. Contr. Dyn.*, Vol. 10, No. 1, 1987, pp. 61–66.

[8] Williams, D., Friedland, B., and Madiwale, A., "Modern Control Theory for Design of Autopilots for Bank-to-Turn Missiles," *AIAA J. Guid. Contr. Dyn.*, Vol. 10, No. 4, 1987, pp. 378–386.

[9] Nesline., F. W., and Zarchan, P., "Optimal Intercept Missile Guidance Strategies with Autopilot Lag," *Proc. Guid. Nav. Contr. Conf.*, 2010. AIAA 2010-7875.

[10] Lee, C., Kim, T., Tahk, M., and Whang, I., "Polynomial Guidance Laws Considering Terminal Impact Angle and Acceleration Constraints," *IEEE Trans. Aero. Elect. Sys.*, Vol. 49, No. 1, 2013, pp. 74–92.

[11] Kim, T.-H., Lee, C.-H., Jeon, I.-S., and Tahk, M.-J., "Augmented Polynomial Guidance With Impact Time and Angle Constraints," *IEEE Tran. Aero. Electro. Sys.*, Vol. 49, No. 4, 2013, pp. 2806–2817.

[12] Tahk, M., Moon, G., and Shim, S., "Augmented Polynomial Guidance with Terminal Speed Constraints for Unpowered Aerial Vehicles," *I. J. Aero. Space Sci.*, Vol. 20, No. 1, 2019, pp. 183–194.

[13] Kwon, W., and Han, S., *Receding Horizon Control: Model Predictive Control for State Models*, Springer, 2006.

[14] Camacho, E. F., and Bordons, C., *Model Predictive Control*, 2nd ed., Springer, 2007. doi:10.1007/978-0-85729-398-5.

[15] Di Cairano, S., and Kolmanovsky, I. V., "Real-Time Optimization and Model Predictive Control for Aerospace and Automotive Applications," *Proc. Amer. Contr. Conf.*, 2018, pp. 2392–2409. doi:10.23919/ACC.2018.8431585.

[16] Eren, U., Prach, A., Koçer, B. B., Raković, S. V., Kayacan, E., and Açıkmeşe, B., "Model predictive control in aerospace systems: Current state and opportunities," *Journal of Guidance, Control, and Dynamics*, Vol. 40, No. 7, 2017, pp. 1541–1566. doi:10.2514/1.G002507.

[17] Zhao, J., Zhou, S., and Zhou, R., "Distributed time-constrained guidance using nonlinear model predictive control," *Nonlinear Dynamics*, 2015, pp. 1399–1416. doi:10.1007/s11071-015-2578-z.

[18] Li, Z., Xia, Y., Su, C.-Y., Deng, J., Fu, J., and He, W., "Missile Guidance Law Based on Robust Model Predictive Control Using Neural-Network Optimization," *IEEE Transactions on Neural Networks and Learning Systems*, Vol. 26, No. 8, 2015, pp. 1803–1809. doi:10.1109/TNNLS.2014.2345734.

[19] Bhattacharjee, D., Chakravarthy, A., and Subbarao, K., "Nonlinear Model Predictive Control based Missile Guidance for Target Interception," *AIAA Scitech*, 2020. AIAA 2020-0865.

[20] Cohen, M. N., "An overview of radar-based, automatic, noncooperative target recognition techniques," *IEEE Int. Conf. Sys. Eng.*, 1991, pp. 29–34.

[21] Wong, S., "Non-cooperative target recognition in the frequency domain," *IEE Proceedings - Radar, Sonar and Navigation*, Vol. 151, 2004, pp. 77–84.

[22] Schiller, J., "Capabilities, Developments and Challenges in Non-Cooperative Target Identification Using Radar ," *Microwaves, Radar and Remote Sensing Symposium*, Kiev, Ukraine, 2011, pp. 24–27.

[23] López-Rodríguez, P., Escot-Bocanegra, D., Fernández-Recio, R., and Bravo, I., "Non-Cooperative Target Recognition by Means of Singular Value Decomposition Applied to Radar High Resolution Range Profiles," *Sensors*, Vol. 15, No. 1, 2015, pp. 422–439.

[24] Nesterov, Y., *Introductory Lectures on Convex Optimization: A Basic Course*, Springer, New York, 2004.

[25] Anderson, J. D., *Aircraft Performance and Design*, McGraw-Hill, 2012.